PRIFYSGOL BANGOR UNIVERSITY 1884

Wideband complex-enhanced chaos generation using a semiconductor laser subject to delay-interfered self-phase-modulated feedback

Zhao, Anke; Jiang, Ning; Xue, Chenpeng; Tang, Jianming; Qiu, Kun

Optics Express

Published: 01/04/2019

Peer reviewed version

Cyswllt i'r cyhoeddiad / Link to publication

09. Oct. 2020

Wideband complex-enhanced chaos generation using a semiconductor laser subject to delay-interfered self-phase-modulated feedback

ANKE ZHAO,[1] NING JIANG,[1,2,*] SHIQIN LIU,[1] CHENPENG XUE,[1,2] JIANMING TANG,[2] AND KUN QIU[1]

[1]School of Information and Communication Engineering, University of Electronic Science and Technology of China, 2006 Xiyuan Avenue, Chengdu 611731, China
[2]School of Electronic Engineering, Bangor University, Dean Street LL57 1UT, Bangor, UK
*uestc_nj@uestc.edu.cn

Abstract: A wideband complexity-enhanced chaos generation scheme is proposed by using semiconductor laser subject to delay-interfered self-phase-modulated optical feedback. The influences of feedback strength, phase modulation index and interference delay on the effective bandwidth and time-delay-signature (TDS) characteristics of the proposed scheme-generated chaos are extensively investigated both experimentally and numerically. The results demonstrate that with the joint effects of phase modulation-induced spectrum expansion and nonlinear filtering of delayed interference, wideband chaos with flat spectrum and excellent TDS suppression characteristics can be generated over a wide dynamic operation range. In comparisons with the relevant chaos generation schemes under convention optical feedback, individual self-phase modulated optical feedback, and delay-interfered optical feedback, the proposed scheme can not only significantly enhance the effective bandwidth of chaos, but also considerably enhance the complexity of chaos by suppressing the TDS towards a distinguishable level close to 0.

1. Introduction

All-optical chaos generation based on external-cavity semiconductor lasers (ECSLs) has drawn great attention because of its potential applications in secure optical communications [1-6], true random bit generation (RBG) [7-15] and chaotic radar [16, 17]. Since in conventional ECSL-based chaos generation systems, chaotic intensity oscillation is often dominated by the intrinsic relaxation oscillation of the laser, in the radio frequency (RF) spectrum of the chaotic signal, the majority of the energy is thus concentrated in the vicinity of the relaxation oscillation frequency. As a direct result, the effective bandwidth is typically a few GHz only. This restricts the signal transmission capacity of optical chaos-based secure communication systems, the rate of RBG and the resolution of radar. On the other hand, since the conventional feedback light is a linear replica of the laser output, the external cavity resonation introduces a periodicity in the chaos, which results in an obvious time delay signature (TDS) that indicates the feedback delay time of the external cavity. The TDS can be easily identified by several methods, such as the calculations of autocorrelation function (ACF), digital mutual information (DMI), and permutation entropy (PE) [18-21]. The obvious TDS degrades the randomness of RBG, threats the privacy of chaos sources in secure communication applications, and degrades the precision of chaotic radar. Therefore, it is vital to explore new chaos generation schemes that support simultaneous bandwidth enhancement and efficient TDS suppression.

To achieve the aforementioned objective, several methods have been proposed in recent years [22-34]. In terms of optical chaos bandwidth enhancement, use can be made of optical injection [22-24], fiber ring resonator with chaos injection [25] and delayed self-interference

[26]. In terms of chaos TDS suppression, use can be made of dual optical feedback [27], grating optical feedback [28, 29] and phase-modulated optical feedback [30]. In particular, a few demonstrations of simultaneous bandwidth enhancement and TDS suppression have also been reported by utilizing optical heterodyning [31], electronic heterodyning [32], optical lens and self-phase-modulated feedback with microsphere resonator [33,34].

From a different perspective, in this work we experimentally and numerically demonstrate a scheme enabling the generating of wideband complexity-enhanced chaos, by making use of electro-optic phase modulation (PM) and delayed interference in the feedback loop of an ECSL. Both of experimental and simulation results indicate that significant bandwidth enhancement and efficient TDS suppression are simultaneously achievable in the proposed scheme.

2.   Experimental setup
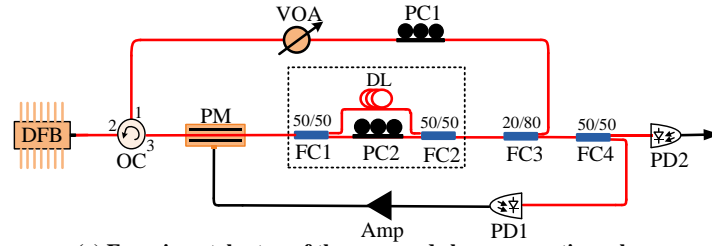
(a) Experimental setup of the proposed chaos generation scheme
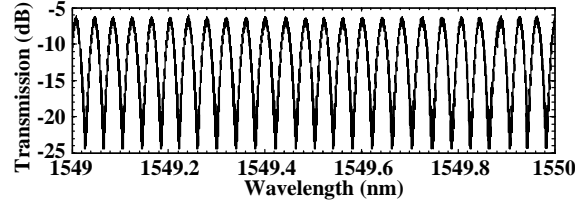
(b) Transmission spectrum of MZI in the experiment

Fig. 1. (a) Experimental setup of the proposed scheme, (b) transmission spectrum of MZI. DFB, distributed-feedback laser; PM, electro-optic phase modulator; OC, optical circulator; PC, polarization controller; FC, fiber coupler; PD, photodetector; Amp: RF amplifier; DL, optical delay line; VOA, variable optical attenuator.

The experimental setup of the proposed wideband complexity-enhanced chaos generation scheme is shown in Fig. 1(a). An external-cavity distributed-feedback (DFB) laser is adopted as a chaos source. Different to the conventional optical feedback (COF), the output of the DFB laser is firstly modulated by an electro-optic phase modulator (Eospace, PM-DS5-20-PFA-PFA-LV, 20 GHz bandwidth) after passing through an optical circulator (OC). Then, the phase-modulated light propagates through a Mach-Zehnder interferometer (MZI) consisting of two 3-dB fiber couplers (FC1 and FC2) and a fiber delay line (DL), which performs the delayed interference. After that, the output of MZI is split by a 20/80 fiber coupler FC3: 20% of the tapped light is sent back into the DFB laser, while the remaining 80% is further split equally by a 50/50 fiber coupler FC4. A variable optical attenuator (VOA) and a polarization controller (PC1) are utilized to adjust the feedback strength and the polarization state of the feedback light, respectively. One part of the tapped light of FC4 is converted into an electronic signal via a photodetector PD1 (u^{2}t, MRV1332A, 30 GHz bandwidth), the electronic signal is then amplified by a RF amplifier (Mini-Circuit, ZVE-3W-183+) and used as the driving signal of the phase modulator. The other part of the tapped light of FC4 is detected by a second wideband photodetector PD2 (u^{2}t, XPDV2120RA, 50 GHz bandwidth) for signal analyzing in the time and frequency domains. In our experimental measurements, the DFB laser operates with a bias current of 19mA which, without any feedback, corresponds to an output power about 2.0 mW and a relaxation oscillation frequency (f_{RO}) of 6.5 GHz. The half-wave voltage of the PM is 4V and the peak amplitude of the chaotic PM driving signal is 4V, which corresponds to a peak

phase shift of π. The bias current and temperature of the DFB laser are monitored by a current-temperature controller (Newport, LDC-3900), and the central wavelength of the DFB laser output is 1549.5nm. The length difference of the two branches of the MZI is 4cm, which corresponds to a delay interference of 0.2ns and has a periodic nonlinear transmission spectrum shown in Fig. 1(b). The length of the feedback loop with the shorter branch of the MZI is 28.8 m, which corresponds to a feedback delay of 144.7 ns (144.9 ns for the longer branch loop). The electronic chaotic signal is measured by a digital oscilloscope (LeCroy, SDA 830Zi-A, 30 GHz bandwidth, 80 GS/s) and its RF spectrum is observed with a RF spectrum analyzer (Rohde & Schwarz, FSW43, 43GHz bandwidth). To highlight the advantages of the proposed scheme, comparisons are made between the proposed scheme and three other relevant chaos generation schemes using ECSLs subject to COF, individual SPMOF (the proposed scheme but without MZI), COF+MZI (the proposed scheme but without phase modulation), in our experimental and numerical investigations.

3.   Experimental results and discussions

For the chaos generated in the abovementioned four scenarios, Fig. 2 shows the corresponding experimental results in terms of the time series, RF spectra, and ACF traces. Here the feedback strength is defined as the power ratio between the feedback light and the laser output, and the feedback strength is chosen as -25 dB. To quantify the bandwidth characteristic of chaos, we adopt the effective bandwidth that is defined as the span between the direct current (DC) components and the frequency where 80% of energy is contained in the RF spectrum [35,36]. For the COF and SPMOF cases, the energy in the RF spectra is mainly concentrated near the relaxation oscillation frequency, and the corresponding effective bandwidths of the chaos generated under these two scenarios are 7.8 GHz and 9.3 GHz, respectively. For the COF+MZI case, it is seen that the relaxation oscillation is eliminated because of the nonlinear filtering effect of the MZI [26]. However, the energy in the RF spectrum degrades quickly with increasing frequency, which results in the effective bandwidth is 8.8 GHz only. While in the proposed SPMOF+MZI scheme, due to phase modulation, there exists many newly-generated frequency components in the feedback light, which expands the spectrum of the phase chaos generated by the ECSL, and then the nonlinear filtering effect of MZI converts the spectrum expansion in the phase chaos into intensity [26,33]. Consequently, with the joint effects of the SPMOF and the MZI, the RF spectrum of chaos becomes much flatter with respect to the other three cases, as such the effective bandwidth is enhanced to 27.9 GHz which is about three times those generated in other three cases.

On the other hand, the TDS characteristics are also shown in the third row of Fig. 2. In the COF case, a large peak appearing at the position of the feedback delay as shown in Fig. 2(a3), suggesting that the TDS is rather easy to be identified. In the cases of both the SPMOF and the COF+MZI, due to the nonlinearity of the PM and the nonlinear filtering effect of the MZI, the linearity of the feedback light in these two cases is degraded, and the periodicity in the chaos is thus degraded correspondingly. For this reason, the TDS is suppressed to some extent, with respect to the COF case. However, the TDS in these two cases is still distinguishable as shown in Figs. 2(b3) and 2(c3). While in the proposed SPMOF+MZI case, as shown in Fig. 2(d3), with the joint nonlinearity effects of the SPMOF and the MZI, the TDS is completely suppressed, no distinguishable peak appears at the position near the feedback delay in the ACF trace, this indicates that the complexity of chaos is greatly enhanced in comparison with all other three cases [36].
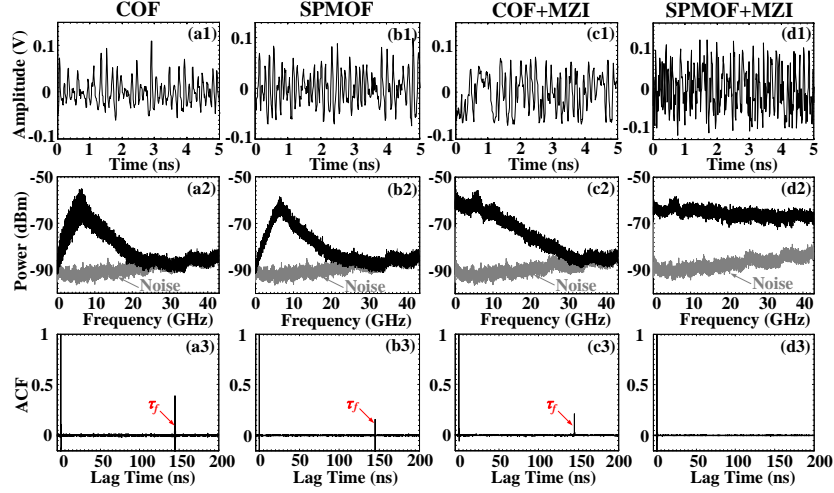
Fig. 2. Experimental time series, RF spectra and ACF traces of chaos generated in the cases of COF (first column), SPMOF (second column), COF+MZI (third column) and the proposed SPMOF+MZI (fourth column). The feedback strength is fixed to -25dB.

Figure 3 shows the experimental results in terms of the temporal waveforms, RF spectra, and ACF traces of chaos generated in the proposed scheme with different feedback strengths. For the weak feedback case with a strength of -30 dB (see Figs. 3(a1)-3(a3)), the RF spectrum is flat over the whole frequency range of the spectrum analyzer, and the effective bandwidth is 29.3 GHz. While in the cases of strong feedback with strengths of -20dB and -15dB, as shown in Figs. 3(b2) and 3(c2), there are a few periodic peaks occurring in the RF spectra, this is due to that the MZI is a periodic nonlinear filter [37]. Since the energy concentrated in these periodic peaks is higher than the flat spectral region, the effective bandwidth is thus degraded to some extent. The effective bandwidths for these two cases are 27.5GHz and 25.1GHz, respectively. Moreover, it is also worth noting that when the feedback strength is sufficiently strong, due to the appearance of the periodic peaks in the RF spectrum of chaos, the TDS in ACF trace is distinguishable as shown in Fig. 3(c3).
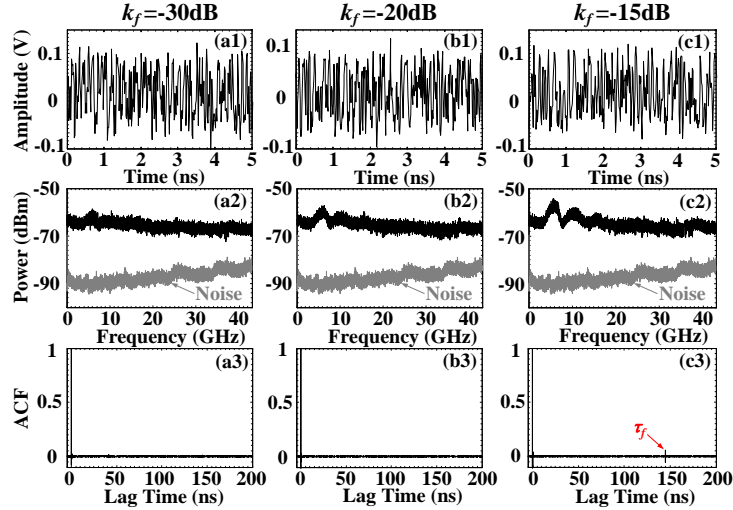

Fig. 3. Experimental time series, RF spectra and ACF traces of chaos generated in the proposed scheme with feedback strengths of -30dB, -20dB and -15dB.

To provide an insight into the dynamic characteristics of the bandwidth and complexity of chaos generated in the proposed scheme, Fig. 4 presents the feedback strength-dependent behaviors of the effective bandwidth and the TDS value in ACF trace, for the four chaos generation cases. Here the TDS value is defined as the maximum value in the vicinity of the feedback delay position in the ACF trace. As shown in Fig. 4(a), the effective bandwidths of chaos in the cases of the COF, the COF+MZI and the SPMOF show very similar developing trends: gradually growing with increasing feedback strength. While in the proposed scheme, the effective bandwidth is slightly reduced from 29.3GHz to 24.1GHz, as the feedback strength increases from -30dB to -10dB. However, it is seen that the effective bandwidth of chaos in the proposed scheme is always wider than those of the other three cases. On the other hand, as shown in Fig. 4(b), the developing trends of complexity (TDS value in ACF trace) in the cases of the COF, the COF+MZI and the SPMOF are also similar, the TDS values firstly decrease with increasing feedback strength, and then gradually increasing with increasing feedback strength. While in the proposed SPMOF+MZI scheme, when the feedback strength is smaller than -18dB, the TDS value is maintained at a low level close to 0, since the TDS can be completely suppressed over this range. When the feedback strength is larger than -18 dB, the TDS value gradually increases to a distinguishable level, but it always remains at a much lower level than those of other three cases, this indicates that the complexity of chaos in the proposed scheme is always enhanced with respect to other three cases. The above results indicate that the proposed scheme can significantly enhance both bandwidth and complexity of chaos, with respect to other three cases.
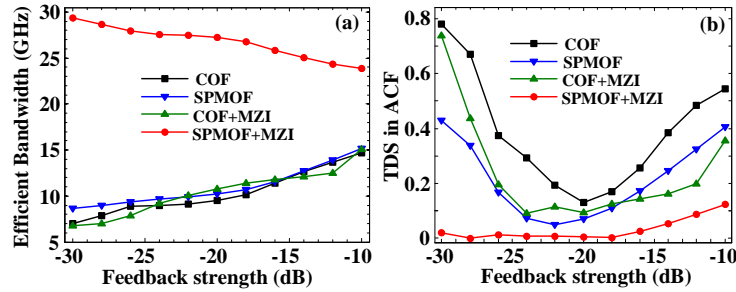

Fig. 4. Experimental (a) effective bandwidth and (b) TDS values in the ACF traces of chaos generated in the cases of COF (square), SPMOF (lower-triangle), COF+MZI (upper-triangle) and SPMOF+MZI (circle), as a function of the feedback strength.

Considering interference delays of 0.1ns, 0.2ns and 1ns, Fig. 5 shows the experimentally measured time series, RF spectra and ACF traces of the corresponding chaotic signals generated in the proposed scheme. In these three cases considered, similar phenomena are observed, wideband chaotic signals with flat RF spectra are always obtainable, the effective bandwidths for these three cases are 30GHz, 29.3GHz and 29.6GHz, respectively. Simultaneously, in all of these three cases, the TDSs are completely suppressed. The results indicate that the prominent bandwidth enhancement and excellent TDS suppression are not affected by the interference delay of MZI. This statement is also confirmed in the following numerical investigations.
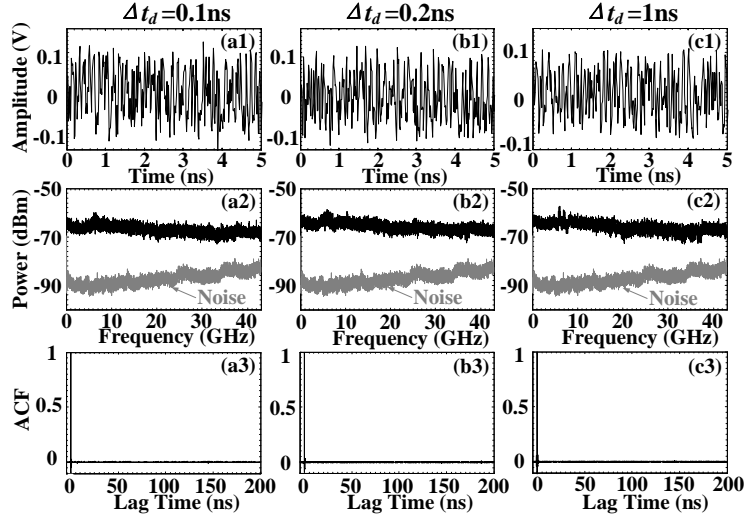
Fig. 5. Experimental time series (first column), RF spectra (second column) and ACF traces (third column) of chaos generated by the proposed SPMOF+MZI scheme, with different interference delays of (a) 0.1ns, (b) 0.2ns and (c) 1ns. The feedback strength is fixed to -30dB.

4. Theoretical model and numerical simulations

In the experiment, due to the limitations of practical dynamic device operation ranges including, device bandwidths (e.g. PD, RF analyzer, RF amplifier), resolution of interference delay of MZI, and gain of the RF amplifier, etc., it is difficult to explore the properties of the proposed scheme over a wide range. To solve such an issue, numerical investigations are performed and presented in this section.

4.1 Theoretical model

The dynamics of the ECSL in the proposed scheme are described by the modified Lang–Kobayashi rate equations, by taking into account self-phase modulation and delay-interfered optical feedback [21-23,27,38]. The rate equations of the slowly-varying complex electric field E and the corresponding carrier number N in the active region of the ECSL are written as:

$$\frac{dE(t)}{dt} = \frac{1+i\alpha}{2}\left[\frac{g\left(N(t)-N_0\right)}{1+\varepsilon|E(t)|^2} - \frac{1}{\tau_p}\right]E + \frac{k_f}{2\tau_{in}}\left[E\left(t-\tau_f\right)\exp\left(i2\pi\omega_0\tau_f + i\varphi\left(t-\tau_f\right)\right)\right.$$
$$\left. + E\left(t-\tau_f-\Delta t_d\right)\exp\left(i2\pi\omega_0\left(\tau_f+\Delta t_d\right) + i\varphi\left(t-\tau_f-\Delta t_d\right)\right)\right] + \sqrt{2\beta N(t)}\chi(t), \tag{1}$$

$$\frac{dN(t)}{dt} = \frac{I}{q} - \frac{N(t)}{\tau_e} - \frac{g\left(N(t)-N_0\right)}{1+\varepsilon|E(t)|^2}|E(t)|^2, \tag{2}$$

$$\varphi(t) = K_{PM}\mathbf{N}\left(\left|E\left(t-\Delta t\right)\right|^2\right)\pi, \tag{3}$$

where k_f denotes the strength of optical feedback defined as the power ratio between the feedback light and the laser output light, τ_f is the delay of the feedback loop of the short branch of the MZI, Δt_d is the interference delay of the MZI, $q=1.6\times10^{-19}$ C is the electron charge, α is the linewidth-enhancement factor, g is differential gain coefficient, ε is the nonlinear gain saturation coefficient, N_0 is the transparency carrier number, I is the bias current, ω_0 is the angular frequency, τ_p is the photon lifetime, τ_e is the carrier lifetime, and τ_{in} is the round-trip time of laser cavity. $\chi(t)$ is a white Gaussian noise with zero mean and unity variance, it is used

to model the spontaneous-emission noise. $\varphi(t)$ is the phase-shift induced by the SPMOF, which is defined in Eq. (3), wherein K_{PM} is the phase modulation index, $\mathbf{N}(|E(t-\Delta t)|^2)$ stands for the normalized electronic PM driving signal, Δt is the delay of the driving signal, which is induced by the photovoltaic conversion and the transmissions of the cable and fiber.

In our simulations, the rate equations are solved by the fourth-order Runge-Kutta algorithm. The operation wavelength is λ=1550 nm, the bias current I is set at I=2I_{th}, where I_{th}=14.7mA is the threshold current of the laser. The intrinsic parameter values of the ECSL are chosen to be their typical values reported in [34,39,40]: α=5, ε=5×10^{-7}, τ_p=2ps, τ_e=2ns, g=1.5×10^{-8}ps^{-1}, N_0=1.5×10^8, τ_{in}=3ps, and β=1.5×10^{-6}ns^{-1}. Unless otherwise stated in the corresponding text, the PM index is set at K_{PM}=1.5, the delay of the PM driving signal is set at Δt=5ns. Meanwhile, similar to that in the experimental setup, the interference delay Δt_d is set at 0.2ns, and the delay of the feedback loop of the shorter (longer) branch of the MZI is τ_f=144.7ns (144.9ns).

4.2 Numerical results

Firstly, we discuss the dynamic behaviors of the ECSL in the proposed scheme. For the purpose of comparison, Figure 6 shows the bifurcation maps of the ECSLs under the aforementioned four chaos generation scenarios. Under the scenario of the COF, as that shown in Fig. 6(a), the state of the ECSL changes from stable to quasiperiodic (multiple periodic) at the feedback strength of about -41dB, and further develops towards chaotic at the feedback strength of -34dB. For the case of the SPMOF (Fig. 6(b)), the bifurcation point occurs at -46dB, and then the ECSL gradually reaches into chaotic regimes when further increasing feedback strength. For the case of the MZI+COF (Fig. 6(c)), the state of the ECSL gets into strong chaotic (the amplitude of chaos fluctuates significantly over a wide dynamic range), when the feedback strength is larger than -34 dB. Nevertheless, in the proposed scheme (Fig. 6(d)), it is shown that the ECSL can easily work in the strong chaotic regimes, even when the feedback strength is as small as -50dB, the output of the ECSL is still chaotic. Therefore, wideband and complexity-enhanced chaotic signals are obtainable in the proposed scheme.
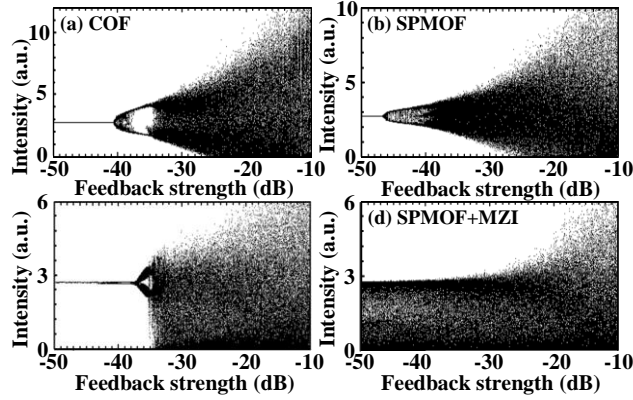

Fig. 6. Bifurcation diagrams with peak-to-peak intensity of chaos generated under the scenarios of (a) COF, (b) SPMOF, (c) COF+MZI and (d) SPMOF+MZI, as a function of feedback strength.

Figure 7 shows the numerical results in terms of time series, power spectra and ACF traces of the chaos generated in the considered four cases with a feedback strength of -25 dB. Similar to the experimental results shown in Fig. 2, the energy in the RF spectra of the chaos generated in the cases of the COF and the SPMOF is mainly concentrated near the relaxation oscillation frequency, and consequently the effective bandwidths of these two cases are only 9.7 GHz and 12.9 GHz, respectively. For the COF+MZI case, although the energy concentration in the vicinity of the relaxation oscillation frequency is eliminated, the energy distribution quickly lowers for high frequency, leading to an effective bandwidth of 11.2 GHz only. Nevertheless, in the proposed SPMOF+MZI case, the RF spectrum is much flatter than those in other three

cases, the energy distribution is almost uniform, and the effective bandwidth is enhanced to 132.7GHz. Moreover, it is also shown that in the proposed scheme, the TDS is completely suppressed and indistinguishable in the ACF trace. The numerical results agree very well with the experimental results. From the numerically-simulated results, it can be predicted that the proposed scheme can generate wideband flat-spectrum chaos with an effective bandwidth beyond 100 GHz and completely-compressed TDS characteristic.
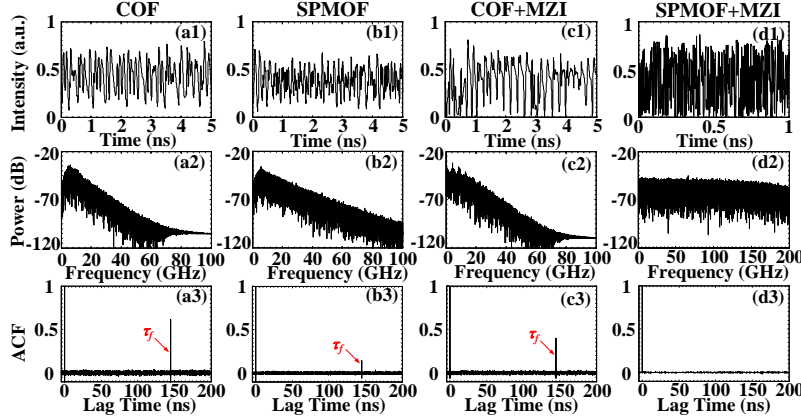

Fig. 7. Numerical time series (first row), RF spectra (second row) and ACF traces (third row) of chaos generated in the cases of (a) COF, (b) SPMOF, (c) COF+MZI and (d) SPMOF+MZI. The feedback strength is fixed to -25dB.

Figure 8 presents the simulated feedback strength-dependent dynamics behaviors of the effective bandwidth and the TDS value in ACF trace for the four chaos generation cases. As shown in Fig. 8(a), the effective bandwidth of chaos in the COF, SPMOF and COF+MZI cases gradually increases with increasing feedback strength, while in the proposed SPMOF+MZI scheme it just slightly decreases. Nevertheless, even in the strong feedback cases, the effective bandwidth of chaos in the proposed scheme can be several times larger than those in other three cases. On the other hand, Figs. 8(b) shows that the TDS value in the proposed scheme is much lower than those associated with other three cases at different feedback strengths, and when the feedback strength is weaker than -18 dB, the TDS value is close to 0. Comparisons with the results in Fig. 4 indicate that the simulation results are well in line with the experimental results.
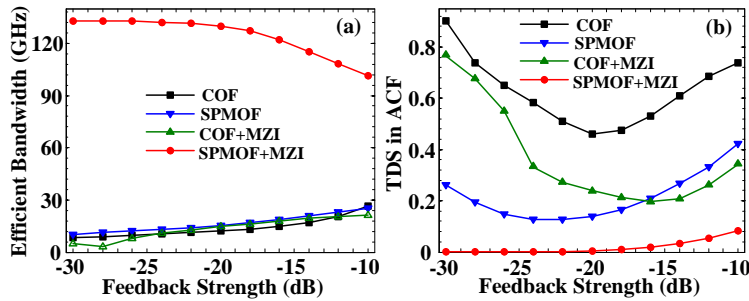

Fig. 8. Numerical results for (a) effective bandwidth and (b) TDS value in ACF trace of chaos generated in the cases of COF (square), SPMOF (bottom-triangle), COF+MZI (upper-triangle) and SPMOF+MZI (circle), as a function of the feedback strength.

To more intuitively analyze the effect of feedback strength on effective bandwidth and TDS for the proposed scheme, Fig. 9 shows the RF spectra and the ACF traces of chaos generated with three representative feedback strengths. Obviously, when the feedback strength is weak, as shown in Fig. 9(a1), the RF spectrum of chaos is flat. While when the feedback is relatively strong, as shown in Figs. 9(b1) and 9(c1), periodic peaks appear in the RF spectra of chaos, due

to the periodic transmissivity of the MZI. Simultaneously, with increasing feedback strength, the signature of interference delay gradually appears in the ACF traces (see the insets of Figs. 9(b2) and 9(c2)), and the TDS value gradually increases to a distinguishable level (see Fig. 9(c2)). It can be easily seen that the simulation results agree well with the experimental results demonstrated in Fig. 3.
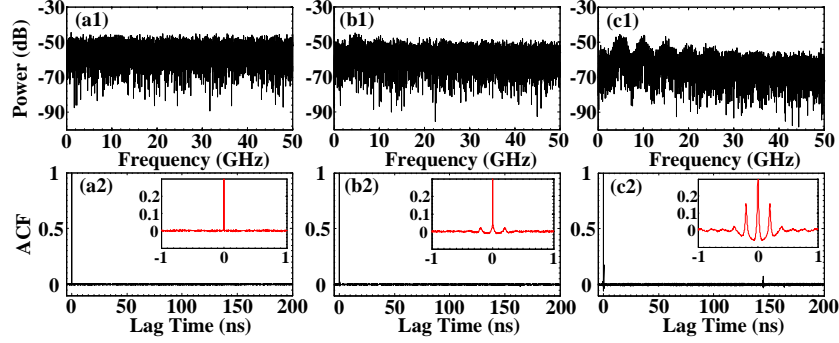

Fig. 9. Numerical results of RF spectra (first row) and ACF traces (second row) of chaos generated in the proposed scheme with feedback strengths of -30 dB (first column), (b) -20 dB (second column) and (c) -10 dB (third column). Insets: the details of ACF traces nearby 0 ns lag.

Furthermore, to extensively investigate the properties of bandwidth enhancement and TDS suppression in the proposed scheme, Fig. 10 shows the influences of the PM index and the feedback strength on the effective bandwidth and the TDS value in ACF trace. As shown in Fig. 10(a), the effective bandwidth developing trends can be classified into two regions with a threshold PM index boundary of about 0.75. When the PM index is smaller than 0.75, the effective bandwidth of chaos increases with increasing feedback strength, the bandwidth enhancement is, however, not significant, as the effective bandwidth is smaller than 40GHz in this region. Nevertheless, when the PM index is larger than 0.75, although the effective bandwidth slightly decreases with increasing feedback strength, the bandwidth enhancement is, however, significant, wideband chaos generation with effective bandwidths beyond 100 GHz can be achieved over a wide operation range. On the other hand, the variation of TDS shown in Fig. 10(b) indicates that for a fixed feedback strength, the larger the PM index, the smaller the TDS value. When the PM index is larger than 1, it is relatively easy to suppress the TDS to an indistinguishable level close to 0. The different variation trends of effective bandwidth over the abovementioned two regions is due to the strength of the spectrum-expansion effect of the SPMOF. When the PM index is small, the spectrum-expansion effect of the SPMOF is not significant, the difference between the SPMOF and the COF is thus not obvious. In such a case, as shown in Figs. 10(c1)-10(c3), the characteristic of chaos in the proposed scheme is similar to that in the case of the COF+MZI, as shown in Figs. 2(c1)-2(c3) and Figs. 7(c1)-7(c3), and the effective bandwidth is enhanced by strong feedback strength, since the RF spectrum becomes flat. Whilst when the PM index is larger than 0.75, the threshold, the spectrum expansion effect of the SPMOF is significant, as shown in Fig. 3 and Fig. 9, as a direct result of the coexistence of the joint effects of the SPMOF and the MZI, the RF spectrum of chaos is flat, and the effective bandwidth is slightly degraded with increasing feedback strength due to the appearance of periodic peaks in the flat RF spectrum. The above discussions indicate that, in the proposed scheme, wideband chaos generation with effective bandwidths beyond 100GHz and efficiently-suppressed TDS can be achieved by using a properly large PM index.
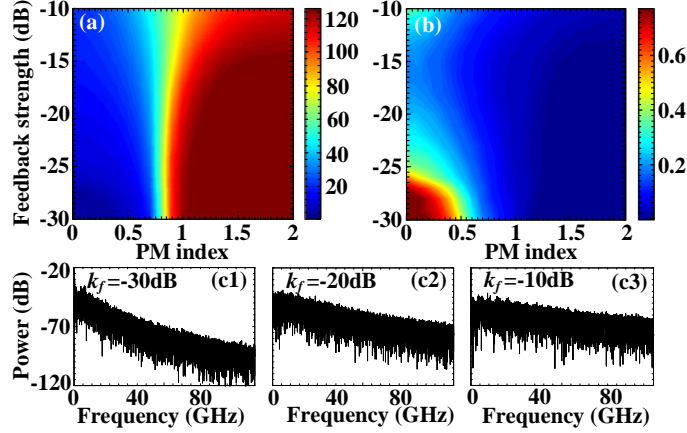
Fig. 10. Influences of PM index and feedback strength on (a) effective bandwidth (GHz) and (b) TDS in ACF in the proposed SPMOF+MZI scheme; (c1-c3) RF spectra of chaos generated in the proposed scheme with a PM index of 0.5. The interference delay is fixed at Δt_d=0.2ns.

In addition, Fig. 11 shows the influences of the delay time (Δt_d) of the MZI and the feedback strength on effective bandwidth and TDS suppression. Apparently, no significant impacts of interference delay on both of bandwidth enhancement and TDS suppression. For a fixed feedback strength, the variations of effective bandwidth and TDS value in ACF are negligible. This means that, the selection of the MZI interference delay in the proposed scheme is flexible, as long as the delay time lager than the coherent time of the laser. In practice, this condition can be easily satisfied by using a sufficiently long delay line in the MZI.
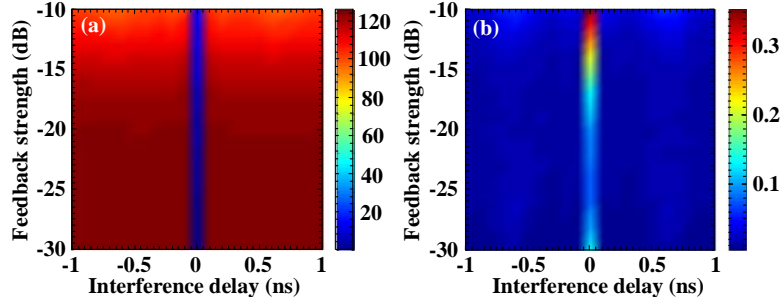

Fig. 11. Influences of interference delay of MZI and feedback strength on (a) effective bandwidth and (b) TDS in ACF trace in the proposed SPMOF+MZI scheme.

5. Conclusions

We proposed and demonstrated a wideband complexity-enhanced chaos generation scheme by introducing self-phase modulation and delayed interference with a MZI into the feedback loop of an ECSL. To demonstrate the effectiveness of the proposed scheme, the investigations were also undertaken of other three relevant chaos generation schemes using ECSLs subject to COF, SPMOF and MZI+COF. The experimental and numerical results indicated that wideband chaos with flat spectrum and efficiently-suppressed TDS is achievable in the proposed scheme. Comparing with other three cases, the proposed scheme can much easily work in the chaotic regimes, the effective bandwidth of chaos can be enhanced significantly and the TDS in chaos can also be efficiently suppressed to an indistinguishable level over a wide dynamic operation range. Moreover, the numerical results indicate that the enhanced effective bandwidth beyond 100 GHz can be obtainable, and that the interference delay does not considerably affect the bandwidth enhancement and TDS suppression properties. The proposed scheme is valuable for

providing wideband chaos sources for applications in secure optical communications, high-speed random bit generation and high-resolution chaotic radar.

Funding

References

1. A. Argyris, D. Syvridis, L. Larger, V. Annovazzi-Lodi, P. Colet, I. Fischer, J. García-Ojalvo, C. R. Mirasso, L. Pesquera, and K. A. Shore, "Chaos-based communications at high bit rates using commercial fibre-optic links," Nature **438**(17), 343–346 (2005).
2. M. Sciamanna, and K. A. Shore, "Physics and applications of laser diode chaos," Nature Photon. **93**(3), 151-162 (2015).
3. J. Ke, L. Yi, G. Xia, W. Hu, "Chaotic optical communications over 100-km fiber transmission at 30-Gb/s bit rate," Opt. Lett. **43**(6), 1323–1326 (2018).
4. N. Jiang, C. Xue, Y. Lv, and K. Qiu, "Physically enhanced wavelength division multiplexing chaos communication using multimode semiconductor lasers," Nonlinear Dynamics **86**(3), 1937-1949 (2016).
5. Y. Fu, M. Cheng, X. Jiang, L. Deng, C. Ke, S. Fu, M. Tang, M. Zhang and D. Liu, "Wavelength division multiplexing secure communication scheme based on an optically coupled phase chaos system and PM-to-IM conversion mechanism," Nonlinear Dynamics **94**(3), 1949-1959 (2018).
6. N. Jiang, A. Zhao, S. Liu, C. Xue, and K. Qiu, "Chaos synchronization and communication in closed-loop semiconductor lasers subject to common chaotic phase-modulated feedback," Opt. Express **26**(25), 32404-32416 (2018).
7. A. Uchida, K. Amano, M. Inoue, K. Hirano, S. Naito, H. Someya, I. Oowada, T. Kurashige, M. Shiki, S. Yoshimori, K. Yoshimura, and P. Davis, "Fast physical random bit generation with chaotic semiconductor lasers," Nature Photon. **2**(12), 728–732 (2008).
8. I. Kanter, Y. Aviad, I. Reidler, E. Cohen, and M. Rosenbluh, "An optical ultrafast random bit generator," Nature Photon. **4**(1), 58–61 (2010).
9. A. Argyris, E. Pikasis, and D. Syvridis, "Gb/s one-time-pad data encryption with synchronized chaos-based true random bit generators," J. Lightw. Technol. **34**(22), 5325–5331 (2016).
10. X. Tang, Z. Wu, J. Wu, T. Deng, J. Chen, L. Fan, Z. Zhong, and G. Xia, "Tbits/s physical random bit generation based on mutually coupled semiconductor laser chaotic entropy source," Opt. Express **23**(26), 33130–33141 (2015).
11. X. Li, S. Li, J. P. Zhuang, and S. C. Chan, "Random bit generation at tunable rates using a chaotic semiconductor laser under distributed feedback," Opt. Lett. **40**(17), 3970–3973 (2015).
12. M. Virte, E. Mercier, H. Thienpont, K. Panajotov, and M. Sciamanna, "Physical random bit generation from chaotic solitary laser diode," Opt. Express **22**(14), 17271–17280 (2014).
13. R. Sakuraba, K. Iwakawa, K. Kanno, and A. Uchida, "Tb/s physical random bit generation with bandwidth-enhanced chaos in three-cascaded semiconductor lasers," Opt. Express **23**(2), 1470–1490 (2015).
14. P. Li, J. Zhang, L. Sang, X. Liu, Y. Guo, X. Guo, A. Wang, K. Alan Shore, and Y. Wang, "Real-time online photonic random number generation," Opt. Lett. **42**(14), 2699–2702 (2017).
15. N. Li, B. Kim, V. N. Chizhevsky, A. Locquet, M. Bloch, D. S. Citrin, and W. Pan, "Two approaches for ultrafast random bit generation based on the chaotic dynamics of a semiconductor laser," Opt. Express **22**(6), 6634–6646 (2014).
16. C. Cheng, Y. Chen, and F. Lin, "Generation of uncorrelated multichannel chaos by electrical heterodyning for multiple-input–multiple-output chaos radar application," IEEE Photon. J. **8**(1), 1-14 (2016).
17. M. Zhang, Y. Ji, Y. Zhang, Y. Wu, H. Xu, and W. Xu, "Remote radar based on chaos generation and radio over fiber," IEEE Photon. J. **6**(5), 1-12 (2014).
18. D. Rontani, A. Locquet, M. Sciamanna, D. S. Citrin, and S. Ortin, "Time-delay identification in a chaotic semiconductor laser with optical feedback: a dynamical point of view," IEEE J. Quantum Electron. **45**(7), 879–891 (2009).
19. S. Xiang, W. Pan, L. Zhang, A. Wen, L. Shang, H. Zhang, and L. Lin, "Phase-modulated dual-path feedback for time delay signature suppression from intensity and phase chaos in semiconductor laser," Opt. Commun. **324**, 38-46 (2014).
20. M. C. Soriano, L. Zunino, O. A. Rosso, I. Fischer, and C. R. Mirasso, "Time scales of a chaotic semiconductor laser with optical feedback under the lens of a permutation information analysis," IEEE J. Quantum Electron. **47**(2), 252-261 (2011).
21. N. Li, R. M. Nguimdo, A. Locquet, D. S. Citrin, "Enhancing optical-feedback-induced chaotic dynamics in semiconductor ring lasers via optical injection," Nonlinear Dynamics **92**(2), 315-324 (2018).
22. A. Wang, Y. Wang, and H. He, "Enhancing the bandwidth of the optical chaotic signal generated by a semiconductor laser with optical feedback," IEEE Photon. Technol. Lett. **20**(19), 1633–1635 (2008).
23. S. Xiang, W. Pan, B. Luo, L. Yan, X. Zou, N. Li, and H. Zhu, "Wideband unpredictability-enhanced chaotic semiconductor lasers with dual-chaotic optical injections," IEEE J. Quantum Electron. **48**(8), 1069-1076 (2012).

24. N. Li, W. Pan, A. Locquet, and D. S. Citrin, "Time-delay concealment and complexity enhancement of an external-cavity laser through optical injection," Opt. Lett. **40**(19), 4416–4419 (2015).
25. Y. Hong, X. Chen, P. S. Spencer, and K. A. Shore, "Enhanced flat broadband optical chaos using low-cost VCSEL and fiber ring resonator," IEEE J. Quantum Electron. **51**(3), 1200106 (2015).
26. A. Wang, Y. Yang, B. Wang, B. Zhang, L. Li, and Y. Wang, "Generation of wideband chaos with suppressed time-delay signature by delayed self-interference," Opt. Express **21**(7), 8701-8710 (2013).
27. J. Wu, G. Xia, and Z. Wu, "Suppression of time delay signatures of chaotic output in a semiconductor laser with double optical feedback," Opt. Express **17**(22), 20124-20133 (2009).
28. S. Li and S. Chan, "Chaotic time-delay signature suppression in a semiconductor laser with frequency-detuned grating feedback," IEEE J. Sel. Top. Quantum Electron. **21**(6), 541–552 (2015).
29. Z. Zhong, Z. Wu, and G. Xia, "Experimental investigation on the time-delay signature of chaotic output from a 1550 nm VCSEL subject to FBG feedback," Photon. Research **5**(1), 6–10 (2017).
30. C. Xue, N. Jiang, Y. Lv, C. Wang, G. Li, S. Lin, and K. Qiu, "Security-enhanced chaos communication with time-delay signature suppression and phase encryption," Opt. Lett. **41**(16), 3690-3693 (2016).
31. A. Wang, L. Wang, P. Li, and Y. Wang, "Minimal-post-processing 320-Gbps true random bit generation using physical white chaos," Opt. Express **25**(4), 3153-3164 (2017).
32. C. H. Cheng, Y. C. Chen, and F. Y. Lin, "Chaos time delay signature suppression and bandwidth enhancement by electrical heterodyning," Opt. Express **23**(3), 2308-2319 (2015).
33. N. Jiang, A. K. Zhao, S. Q Liu, C. P. Xue, B. Y. Wang, and K. Qiu, "Generation of broadband chaos with perfect time delay signature suppression by using self-phase-modulated feedback and a microsphere resonator," Opt. Letters **43**(21), 5359-5362 (2018).
34. N. Jiang, C. Wang, C. Xue, G. Li, S. Lin and K. Qiu, "Generation of flat wideband chaos with suppressed time delay signature by using optical time lens," Opt. Express **25**(13), 14359-14367 (2017).
35. F. Y. Lin, J. M. Liu, "Nonlinear dynamical characteristics of an optically-injected semiconductor laser subject to optoelectronic feedback," Opt. Commun. **221**(1-3), 173-180 (2003).
36. D. Rontani, E. Mercier, D. Wolfersberger, and M. Sciamanna, "Enhanced-complexity of optical chaos in a lasr diode with phase-conjugate feedback," Opt. Lett. **41**(20), 4637-4640 (2016).
37. C. Li, J. Mao, R. Dai, X. Zhou, J. Jiang, "Frequency-sextupling optoelectronic oscillator using a Mach–Zehnder interferometer and an FBG," IEEE Photon. Technol. Lett. **28**(12), 1356–1359 (2016).
38. R. Lang and K. Kobayashi, "External optical feedback effects on semiconductor injection laser properties," IEEE J. Quantum Electron. **16**(3), 347–355 (1980).
39. A. Bogris, P. Rizomiliotis, K. E. Chlouverakis, A. Argyris and D. Syvridis, "Feedback phase in optically generated chaos: a secret key for cryptographic application," IEEE J. Quantum Electron. **44**(2), 119-124 (2008).
40. D. Kanakidis, A. Argyris, A. Bogris, and D. Syvridis, "Influence of the decoding process on the performance of chaos encrypted optical communication systems," J. Lightw. Technol. **24**(1), 335-341 (2006).